scientific reports

Check for updates

OPEN

Integrated bioinformatics analysis identified cuproptosis-related hub gene Mpeg1 as potential biomarker in spinal cord injury

Dandan Mao[1,5], Qi Chen[2,5], Shuolan Tong[3], Zixia Xu[3], Guofeng Yu[1], Chuan Chang[4]✉ & Yao Lv[1]✉

Spinal cord injury (SCI) is a profound ailment lacking a well-defined molecular mechanism and effective treatments. Cuproptosis, identified as a recently discovered cell death pathway, exhibits diverse roles in various cancers. Nevertheless, its involvement in SCI is yet to be elucidated. Firstly, the RNA sequencing data of 1, 3, 7 dpi SCI samples were collected from GEO database. We performed differential expression analysis on these samples with varying cuproptosis-related scores calculating by ssGSEA. Subsequently, we conducted enrichment analyses with KEGG, GO, and GSEA. Simultaneously, we executed WGCNA analysis using cuproptosis-related scores, selecting the most relevant module for enrichment analysis. Hub genes were identified at the intersection of PPI analysis results from two modules and cuproptosis-related DEGs. Additionally, relying on the immune infiltration landscape associated with cuproptosis, we carried out immune cell correlation analysis on hub genes. Finally, to corroborate our earlier findings, we utilized single-cell RNA-seq analysis and in vitro experimental validation. Based on ssGSEA, differential expression analysis and WGCNA analysis, we identified two modules that were highly relevant to cell division and immune processes, respectively. From these modules, we identified two hub genes, *Cd48* and *Mpeg1*, which exhibited a strong positive correlation ($R = 0.92$) and shared similar pathways. Furthermore, we observed a positive correlation between M2 macrophages and *Cd48/Mpeg1*. To validate our findings, we performed external cohort validation using a single-cell RNA sequencing dataset. The results confirmed that *Mpeg1* was highly expressed in microglia (macrophages in center nervous system) following spinal cord injury. Additionally, we conducted in vitro experiments to further validate the molecular functions of *Mpeg1* in SCI. In summary, targeting *Mpeg1*, as well as cuproptosis and immune cell infiltration, holds promise as a potential strategy for reducing spinal cord tissue damage and promoting recovery after SCI. These findings provide valuable insights for future therapeutic interventions.

Keywords Cuproptosis, Spinal cord injury, WGCNA, Immune infiltration, Single-cell RNA sequencing analysis

Spinal cord injury (SCI) presents a devastating neurological condition, resulting in a spectrum of physiological defects encompassing motor, sensory, and autonomic dysfunction[1]. On a global scale, SCI impacts 20.6 million individuals, with an annual incidence of 250,000 to 500,000 cases[2,3]. SCI is categorized into two types: primary and secondary[4]. Mechanical forces cause the former, while the latter involves multifaceted pathological mechanisms that initiate after primary injury and can persist for weeks[5]. Among them, immune imbalance is one of the important mechanisms. For example, M1 microglial/macrophages infiltration increases the inflammatory response in SCI, inhibiting its repair, while M2-types have the opposite effect[6]. Moreover, newly synthesized myelin is attacked by imbalanced immune cells, leading to inhibited neuronal function[7]. Through the combined action of various cytokines and cells, glial scars gradually form and mature[8,9]. Although medication and surgery are common therapies for SCI, neither can fully restore function to the injured spinal cord. Therefore, a deeper

[1]Department of Neurosurgery, The Quzhou Affiliated Hospital of Wenzhou Medical University, Quzhou People's Hospital, Quzhou, China. [2]Department of Nursing, Huashan Hospital, Fudan University, Shanghai, China. [3]The First Clinical Medical College, Wenzhou Medical University, Wenzhou, China. [4]Department of Neurosurgery, Huashan hospital, Fudan University, Shanghai, China. [5]Dandan Mao and Qi Chen contributed equally to this work. ✉email: changchuan@huashan.org.cn; lvyao20181219@163.com

understanding of the pathological mechanisms of SCI is crucial, along with the exploration of new therapeutic targets and methods.

Cell death constitutes a pivotal pathological process in SCI[10]. Recent studies have uncovered the common involvement of diverse cell death mechanisms, including apoptosis, necrotic apoptosis, autophagy, paraptosis, and pyroptosis, in SCI[11]. In 2022, the Tsvetkov P team[12] proposed a novel copper-dependent cell death pathway termed cuproptosis. The human body necessitates the regulation of copper ion levels within a specific range to meet the requirements of vital life processes[13]. Copper ions play integral roles in numerous physiological processes, such as cell metabolism, the respiratory chain, and ceruloplasmin synthesis[14]. However, excessive levels of copper ions can induce oxidative stress[15], and culminate in cell death[16], contributing to various diseases. Research has disclosed the multifaceted roles of cuproptosis in different cancers, functioning either as a risk factor or a protective factor[17]. Nevertheless, the involvement of cuproptosis in SCI remains unexplored. An investigation observed an upward trend in serum copper concentration within 24 h in SCI patients who did not receive relief intervention, and a strong correlation was found between temporal changes in copper concentration and clinical outcomes of SCI[18]. Elisa Garcia et al. reported the potential therapeutic benefits of supplementing trace elements like vitamin E and copper for individuals with acute SCI, promoting T cell activation and proliferation, ameliorating immune suppression, mitigating complications, and enhancing motor recovery[19]. Hence, the dual impact of copper in SCI, whether protective or deleterious, merits further discussion.

MPEG1 is a type I transmembrane protein located intracellularly and is considered an ancient ancestor of the membrane attack complex/perforin (MACPF) protein family[20]. It exhibits widespread expression in macrophages and serves as a distinctive marker for these cells[21]. *MPEG1* plays a pivotal role in cytophagocytosis, immune regulation, and inflammation. Both human macrophages and neutrophils constitutively express *MPEG1*. In cases of *MPEG1* deficiency, cell phagocytosis becomes impaired, resulting in the observation of pro-inflammatory signals during the inflammatory response, consequently leading to the upregulation of *MPEG1* expression[21]. Additionally, *MPEG1* facilitates the entry of various antimicrobial effectors into cells, and without *MPEG1*, multiple cell lines are vulnerable to bacterial infections[22]. According to Ferrero et al., *MPEG1* is sustainably expressed in mature B lymphocytes and plays a pivotal role in eliminating intracellular bacteria as well as the phagocytosis of scleroid B cells[23]. However, the relationships between *MPEG1* and SCI/cuproptosis still unclear.

In this investigation, we applied single-sample Gene Set Enrichment Analysis (ssGSEA) to compute coproptosis-related scores for the SCI samples. Subsequently, we identified two genes, namely *Cd48* and *Mpeg1*, through a combination of differential gene analysis and Weighted Gene Co-expression Network Analysis (WGCNA). We then conducted comprehensive analyses involving immune infiltration and enrichment related to these two genes, revealing a strong correlation between both genes and M2 macrophage immune infiltration. Moreover, single-cell analysis was performed and *Mpeg1* was identified as hub gene. Finally, in vitro study validated the molecular function of *Mpeg1*. These findings provide valuable insights for SCI.

Materials and methods

Data collection

Four spinal cord injury (SCI) microarray datasets, namely GSE42828, GSE47681, GSE27359, and GSE5296, were sourced from the GEO database (https://www.ncbi.nlm.nih.gov/geo/), utilizing the "GEOquery" package. We employed the "ComBat" function from the "sva" R package to mitigate batch effects and integrate these four datasets. The different datasets were difined as the batch using "model.matrix" function. Principal components analysis (PCA) was performed before and after removing the batch effects. This process involved the exclusion of specially treated mice and any aberrant samples.

ssGSEA

As per the findings of Tsvetkov et al.[12], all cuproptosis-related marker genes have been identified in this study. These cuproptosis-related genes were designated as the reference gene set, and normalized gene expression data were subsequently utilized for conducting single-sample Gene Set Enrichment Analysis (ssGSEA) through the R package "GSVA." Subsequently, the spinal cord injury (SCI) samples were categorized into low- and high-score groups based on the cuproptosis-related scores calculated for each sample.

Differential analysis and WGCNA

The analysis of differential expressed genes (DEGs) between the low- and high-score groups involved the use of the "Limma" R package. A threshold of $|\log2FC| > 1$ and adjusted $P < 0.05$ was applied to identify cuproptosis-related DEGs. Subsequently, the "ggplot2" and "pheatmap" packages were employed to create visual representations in the form of heatmaps and volcano plots.

To facilitate the clustering of genes with similar expression patterns, the Weighted Gene Co-expression Network Analysis (WGCNA) algorithm was utilized. This algorithm was employed to construct gene clustering modules within a co-expression network of cuproptosis-related genes using the "WGCNA" R package. The following steps were executed: Firstly, a soft-thresholding power of 2 was established. Secondly, the adjacency matrix, derived from this soft-thresholding power, was transformed into the topological overlap matrix. Thirdly, genes with high co-expression were grouped into modules based on a hierarchical clustering tree. Finally, module genes displaying the highest correlation, characterized by cuproptosis scores, were identified. Subsequently, these genes were analyzed for protein-protein interactions (PPI) using the STRING database (https://string-db.org) and visualized through Cytoscape software (version 3.9.1). The MCC algorithm within the CytoHubba plug-in was then employed to select the top 30 genes based on their scores and rankings as key nodes within the PPI network[24,25].

Ultimately, after obtaining the cuproptosis-related DEGs and genes from the cluster module using WGCNA, the top 30 genes were selected from each set. Then, the cuproptosis-related hub genes were filtered by identifying the intersection of these two gene lists.

Functional enrichment analysis

To enrich the relevant pathways, Gene Ontology (GO) analysis and Kyoto Encyclopedia of Genes and Genomes (KEGG) analysis were performed using the "clusterProfiler" R package. The GO analysis included three categories: molecular function (MF), cellular component (CC), and biological process (BP). Meanwhile, we performed Gene Set Enrichment Analysis (GSEA) at www.gsea-msigdb.org/gsea/index.jsp to examine meaningful differences between groups. For single-gene GSEA analysis, the samples were divided into *Mpeg1* high-expressed group and *Mpeg1* low-expressed group based on the median expression level of *Mpeg1*, firstly. Then, "Limma" package was used to performed differential analysis, following by GSEA analysis. Adjusted P value < 0.05 was identified as enriched GSEA items. Finally, the top 5 GSEA terms based on adjusted P value were visualized by "enrichplot" package.

Immune cell infiltration analysis

The "IOBR" package was applied to assess immune infiltration, including 7 algorithms: CIBERSORT, ESTIMATE, IPS, MCPCOUNTER, XCELL, QUANTISEQ, MCP and EPIC. The immune infiltration analysis on the SCI samples was conducted using the CIBERSORT algorithm from the "IOBR" package, based on the scores obtained from single-sample Gene Set Enrichment Analysis (ssGSEA). Meanwhile, since CIBERSORT, XCELL, and QUANTISEQ algorithms are commonly used and provide comprehensive immune cell infiltration results, these three methods were selected to investigate the correlation between cuproptosis-related hub genes and immune cell infiltration.

Co-expression analysis of hub genes

To conduct co-expression analysis of the hub genes, we utilized FPKM values to compute pairwise Pearson correlation coefficients between the hub genes and the cuproptosis-related genes. Positive values indicate positive correlations, while negative values signify negative correlations, and larger absolute values denote stronger correlation strength.

Single-cell RNA sequencing analysis

We obtained the single-cell RNA-seq data from a public database (https://doi.org/10.6084/m9.figshare.17702045.v2). This single-cell sequencing data were well processed and annotated. The other analysis was carried out using the Seurat R package (version 4.0.4). For checking the data quality, the following quality control criteria were used: (1) Ensuring a number of detected genes per single cell between > 200 and < 5000; (2) UMI counts within the range of 1000 and 20,000; (3) Maintaining the percentage of mitochondrial genes below 15% of the total expressed genes. Subsequently, to visualize the expression of pivotal genes for each cell type, violin plots and feature plots were utilized.

Spinal cord injury model

All study procedures were performed according to experimental protocols approved by the Animal Ethics Committee of Fudan University (Approval number: 202305010Z). C57BL/6 mice, weighing between 25 and 30 g, were subjected to general anesthesia prior to undergoing a laminectomy. A spinal cord clip injury at the T10 level was then inflicted using a 50-gram forceps for a duration of 10 s. In the postoperative period, prophylactic measures were taken to prevent infection, which included a daily intraperitoneal administration of penicillin for three consecutive days. Additionally, twice-daily bladder massages were performed to assist in urination until the mice regained the ability to void spontaneously. Six mice were assigned per group empirically. The mice were euthanized following an overdose of isoflurane (RWD, China; R510-22-10) anesthesia. After euthanasia, a 0.9% saline solution was used for cardiac perfusion. All experiments were performed in accordance with relevant guidelines and regulations (ARRIVE guidelines).

Hematoxylin-eosin (H&E) staining

Spinal cord sections were deparaffinized sequentially with xylene, anhydrous ethanol, 95% ethanol, 80% ethanol, 70% ethanol, and distilled water. The sections were then stained with hematoxylin for 5 min, rinsed in water to remove excess stain, followed by eosin staining for 1 min. After washing, the sections were treated with 70% ethanol for 10 s, 80% ethanol for 10 s, 90% ethanol for 10 s, anhydrous ethanol for 10 s, and then cleared in xylene for 5 min before being mounted and observed.

Western blot

Post-homogenization and centrifugation, the supernatant was harvested, and protein concentrations were measured with the BCA protein assay kit (P0011, Beyotime, China). Each sample, containing 20 micrograms of protein, was applied to a sodium dodecyl sulfate-polyacrylamide gel for electrophoresis (SDS-PAGE). The resolved proteins were then transferred onto polyvinylidene fluoride (PVDF) membranes at 90 V for 60 min. After blocking to avoid non-specific interactions, the membranes were exposed to the primary anti-FDX1 antibody (Abmart, T510671) overnight at 4 °C. The membranes were rinsed with TBST to eliminate unbound antibodies, and subsequently incubated with a secondary anti-rabbit antibody in blocking buffer for 60 min at ambient temperature. The proteins were finally visualized by an enhanced chemiluminescence (ECL) system (Amersham).

Cell culture
The BV2 microglial cell line, derived from neonatal mouse microglia immortalized with Raf/Myc, was cultured in DMEM medium supplemented with 10% fetal bovine serum (FBS, 12664025, Gibco, USA) and 1% penicillin/streptomycin. The cells were incubated in a CO2 incubator at 37 °C. Upon reaching 80% confluence, cell passaging was carried out using 0.25% trypsin. Subsequently, the microglial cells were exposed to endotoxin (L2630, Sigma-Aldrich, USA) at a concentration of 10 mg/ml.

Real-time quantitative PCR
To extract total RNA from samples of different treatment groups, we employed RNA-quick Purification (ES SCIENCE, Shanghai, China), following the manufacturer's instructions. We then reverse transcribed the RNA samples into cDNA using the HiScript III All-in-one RT SuperMix Perfect for qPCR kit (Vazyme, Nanjing, China). Subsequently, we prepared positive controls and detection samples in a standardized system, and quantified them through amplification simultaneously using Vazyme's reagents under the following reaction conditions: 95 °C for 30 s, followed by 40 cycles of 95 °C for 10 s and 60 °C for 30 s. To determine relative mRNA expression, we normalized it to GAPDH and used the 2-△△Ct method.

MPEG1 forward primer: 5'- CTGGATGATAATAGCGTGTGCT-3', reverse primer: 5'- CAAGACAGGTAG TTTCAGGGC-3'.

GADPH forward primer: 5'-AGCTTCGGCACATATTTCATCTG-3', reverse primer: 5'-CGTTCACTCCCA TGACAAACA-3'.

RNA interference and cell transfection
Small interfering RNAs (siRNAs) designed to target *Mpeg1* with the sequence 5′-CCACCUCACUUUCUAUC AA-3′ were synthesized by BioTNT in Shanghai, China. For the transient transfection process, Lipofectamine RNAiMAX reagent from Thermo Fisher Scientific in Massachusetts, USA, was employed. Subsequent functional assays were initiated 48 h post-transfection to assess the effects of Mpeg1 knockdown.

Elisa
Perform the ELISA by coating the plate with a specific antibody, adding the sample or standard, then a detection antibody, followed by a color-developing enzyme conjugate. Add the substrate to develop color, and measure the absorbance to quantify the target protein. ELISA kits include TNFα (MA0759, Meilunbio, China), IL-1β (MA0751, Meilunbio, China).

Immunofluorescence analysis
Cells were grown on glass slides, fixed with 4% paraformaldehyde, and permeabilized with 0.1% Triton X-100. After blocking, primary antibody (CD86, Abmart, PU885801) were applied overnight at 4 °C, followed by incubation with fluorescently labeled secondary antibody. Nuclei were stained with DAPI, and slides were mounted for visualization under a fluorescence microscope.

Statistical analysis
The R programming language was used for statistical analysis. For comparisons between two conditions, two-sided Student's t tests were used. All statistical analyses were conducted using two-tailed tests, with P values greater than 0.05 considered statistically significant (*P<0.05, **P<0.01, and ***P<0.001).

Results
ssGSEA of cuproptosis
The study design is illustrated in Fig. 1. Firstly, we contrasted the clip SCI model successfully (Fig. 2A). To uncover the cuproptosis level of different time points after SCI, western blot analysis was performed to detect the expressed level of FDX1. The results showed that the cuproptosis was highly enriched in 1, 3, 7 dpi of SCI (Fig. 2B). The original blots were showed in Fig. S1. The four datasets, GSE42828, GSE47681, GSE27359, and GSE5296, were integrated and underwent batch effect correction, and data quality assessments were conducted pre- and post-calibration. The results of the principal component analysis (PCA) (Fig. S2A–B) demonstrated that. Following correction, the samples and gene expression from the four GEO datasets exhibited uniform distribution. Then, 1, 3, 7 dpi samples of SCI were collected from these four datasets.

A total of 343 cuproptosis-related differentially expressed genes (DEGs) were identified through differential analysis of cuproptosis-related scores, consisting of 3 up-regulated genes and 340 down-regulated genes (Fig. 2C). To visualize the expression levels of the cuproptosis-related DEGs, a heat map was generated, displaying the expression levels of the top 30 DEGs with the highest absolute fold changes (Fig. 2D).

Gene functional enrichment analysis of cuproptosis related-DEGs
The KEGG analysis results revealed that the cuproptosis-related DEGs were predominantly enriched in pathways including Natural killer cell-mediated cytotoxicity, Lysosome, Phagosome, and B cell receptor signaling pathway (Fig. 3A). Based on the analysis of BP, the cuproptosis-related DEGs exhibited substantial enrichment in immune-related pathways, such as negative regulation of immune responses, leukocyte promotion, and the regulation of immune effector processes. When considering CC, these DEGs were primarily enriched in collagen trimers, pharmacological vesicles, and immunological synapses. The MF enrichment analysis highlighted significant enrichment of immune receptor activity, cargo receptor activity, and lipoprotein particle binding (Fig. 3B).

Furthermore, the GSEA based on the Hallmark gene set underscored the significant enrichment of pathways like "OXIDATIVE PHOSPHORYLATION" and "P53 Pathway" (Fig. 3C). Employing the KEGG pathway gene set, GSEA suggested the potential involvement of pathways like "ACTION OF THE AP1 FAMILY OF

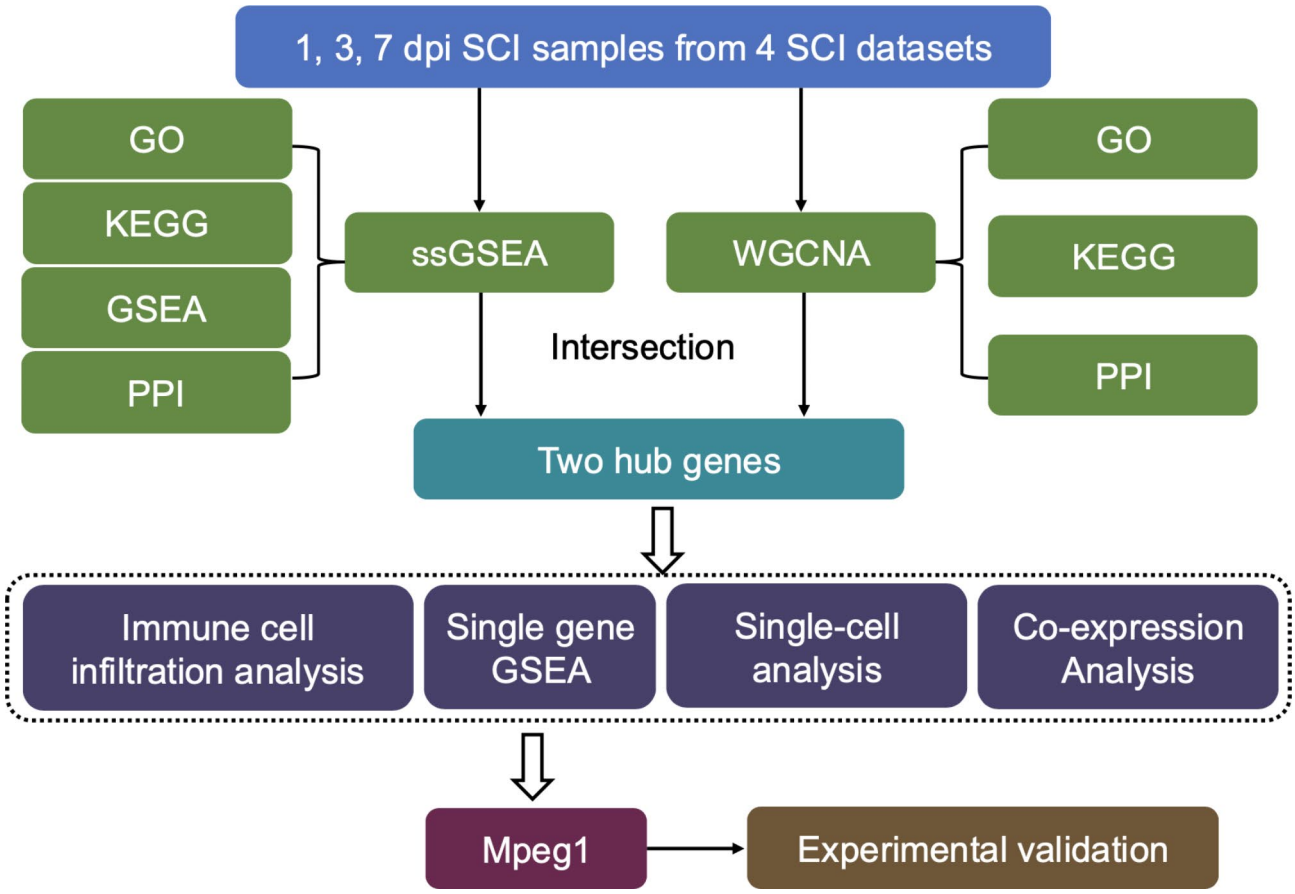

Fig. 1. The study design. dpi: days post injury; SCI: spinal cord injury; GO: Gene Ontology; PPI: protein-protein interaction; KEGG: Kyoto Encyclopedia of Genes and Genomes; GSEA: Gene Set Enrichment Analysis; ssGSEA: single-sample Gene Set Enrichment Analysis; WGCNA: Weighted correlation network analysis.

TRANSCRIPTION FACTORS", "KRESPEL CD99 TARGETS DN" in cuproptosis-related mechanisms in spinal cord injury (Fig. 3D).

Cuproptosis-related gene models of spinal cord injury

The samples with SCI were clustered based on cuproptosis-related scores, and no abnormal samples were found in the cluster tree. A cluster tree containing a phenotypic feature heatmap was then reconstructed (Fig. S3A). Before establishing the expression network, we selected an optimal soft threshold ($\beta = 2$) based on the scale-free topological fitting index and average connectivity (Fig. 4A). Both the histogram and the degree of freedom test confirmed that this selected β threshold effectively established a scale-free gene network (Fig. 4B). The gene modularity-trait correlation was depicted via a heatmap using Spearman correlation coefficients, resulting in the identification of seven gene modules: black, blue, turquoise, green, magenta, brown, and pink (Fig. 4C). The result of combining the cluster tree with the module heat map was presented in Fig. S3B. Among these seven modules, the turquoise module (cor = -0.57, $P = 1e\text{-}08$) and the blue module (cor = -0.53, $P = 3e\text{-}07$), which displayed the most negative correlation with cuproptosis-related scores, were selected for further analysis (Fig. 4D). Scatter plots illustrating the relationship between gene significance and module membership in the turquoise module (Fig. 4E: cor = 0.88, $P = 1e\text{-}200$) and the blue module (Fig. 4F: cor = 0.83, $P = 1e\text{-}200$) demonstrated a significant positive correlation. Heat maps of gene expression in the turquoise and blue modules were also provided (Fig. S3C–D).

Screening of hub genes in spinal cord injury

In our study, we used the MCC algorithm in Cytohubba to conduct PPI analysis on module genes from the two modules and cuproptosis-related DEGs (Fig. 5A). By intersecting the top 30 genes from each of these three analyses, we identified two hub genes: Cd48 and Mpeg1 (Fig. 4G). We conducted GO enrichment analysis on 1,105 module genes in the turquoise module and 1,057 module genes in the blue module. In the blue module, genes were primarily associated with cell division (Fig. 5A), encompassing processes like nuclear division, chromosome segregation, nuclear chromosome segregation, and sister chromatid segregation. On the other hand, the modular genes of turquoise were mainly related to immune processes, such as negative regulation of immune system process, regulation of immune effector process, leukocyte cell – cell adhesion, proliferation,

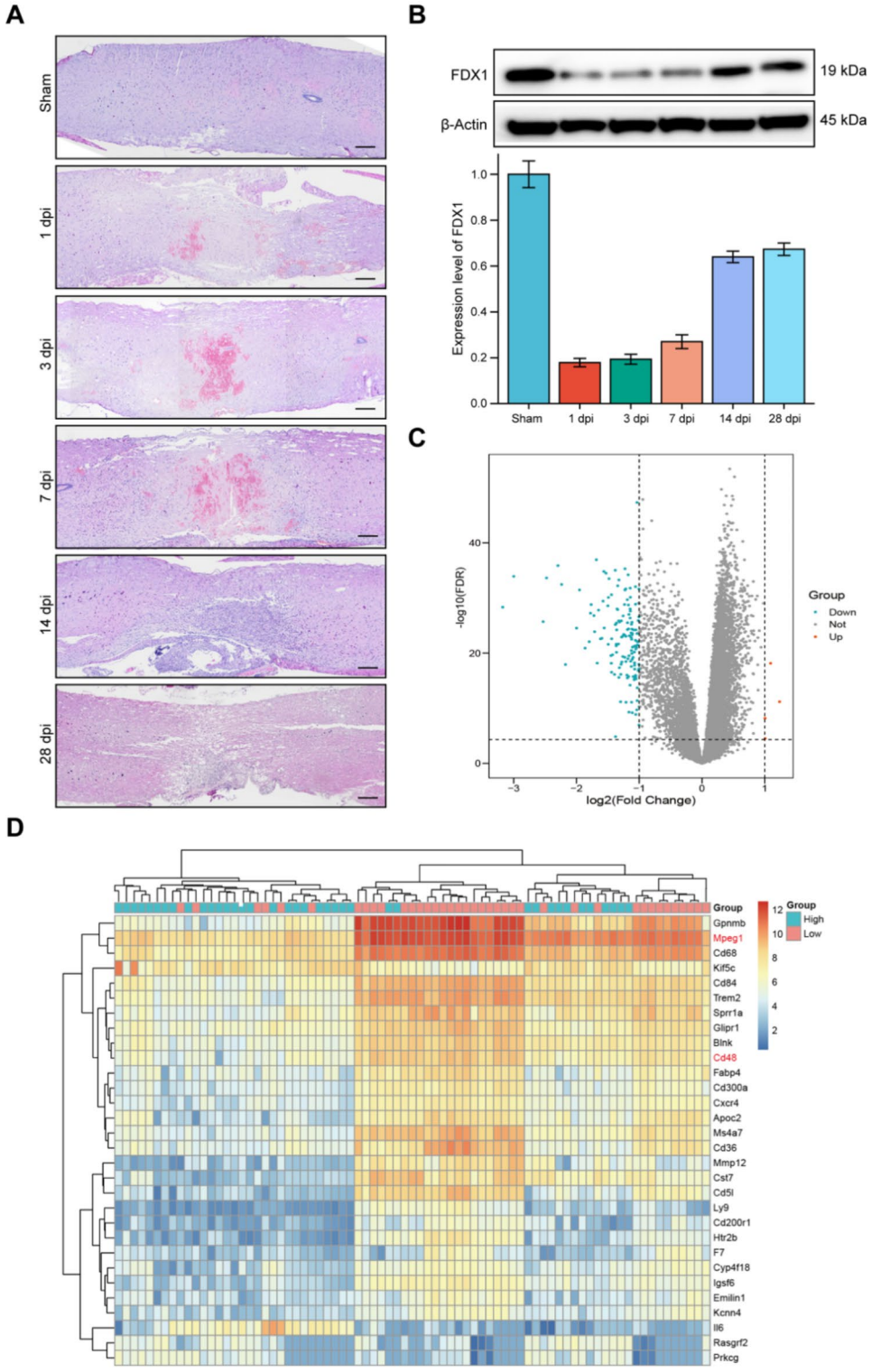

Fig. 2. The results of differential analysis. The results of H&E staining show spinal cord injury (SCI) model is established successfully. (**B**) Western blot analysis of FDX1 level of different time points after SCI (The experiments were repeated three times). Volcano plot (**C**) showed all the cuproptosis-related DEGs and the heatmap (**D**) showed the top 30 DEGs. Abbreviation: dpi, days post-injury.

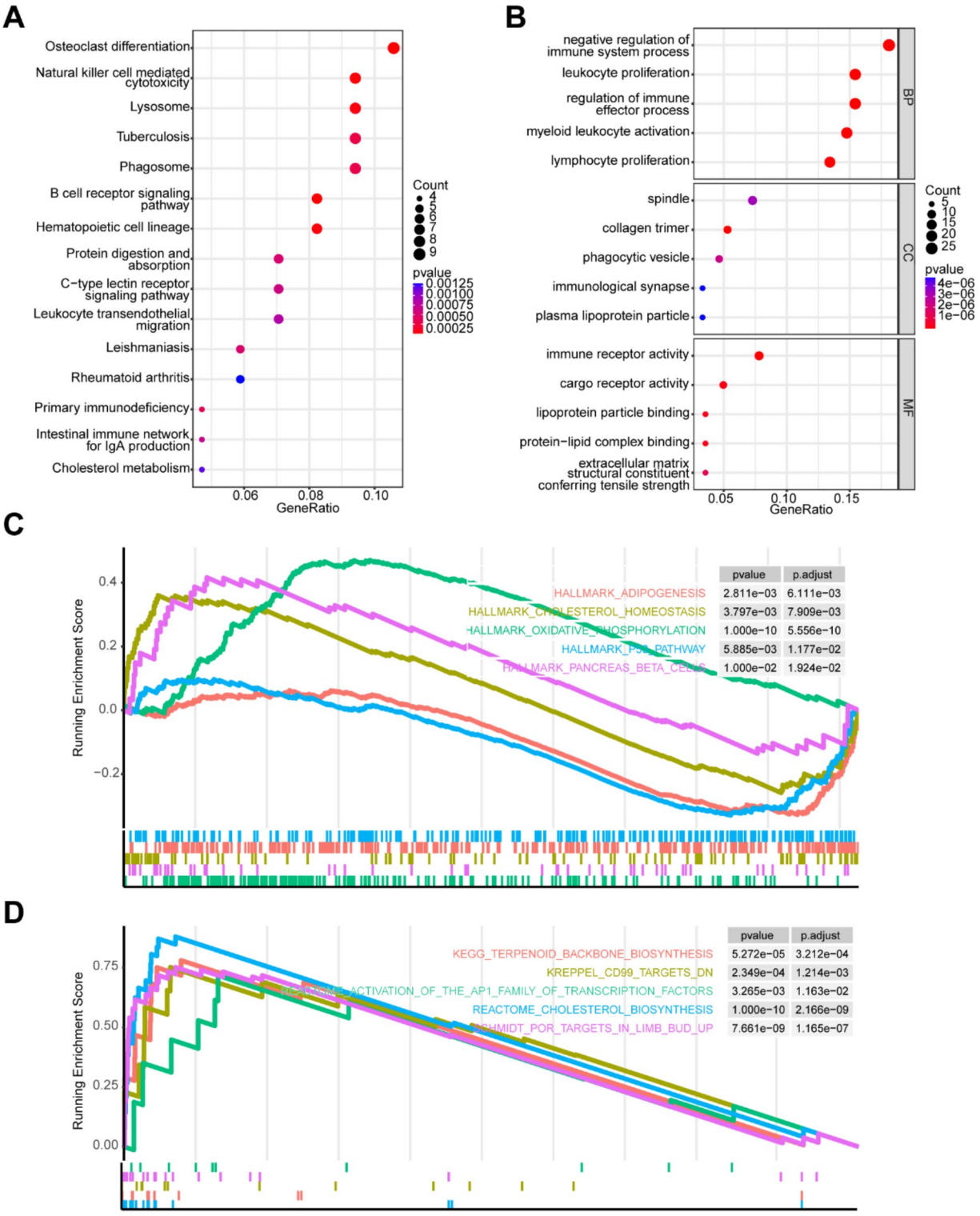

Fig. 3. Functional enrichment analysis of cuproptosis-related DEGs. KEGG (**A**) and GO (**B**) enrichment analysis found immune related pathways were significantly enriched. The results of GSEA enrichment analysis based on the HALLMARK gene set (**C**) and KEGG gene set (**D**), respectively. The KEGG pathways were cited from www.kegg.jp/kegg/kegg1.html. (Copyright permission number: 241602).

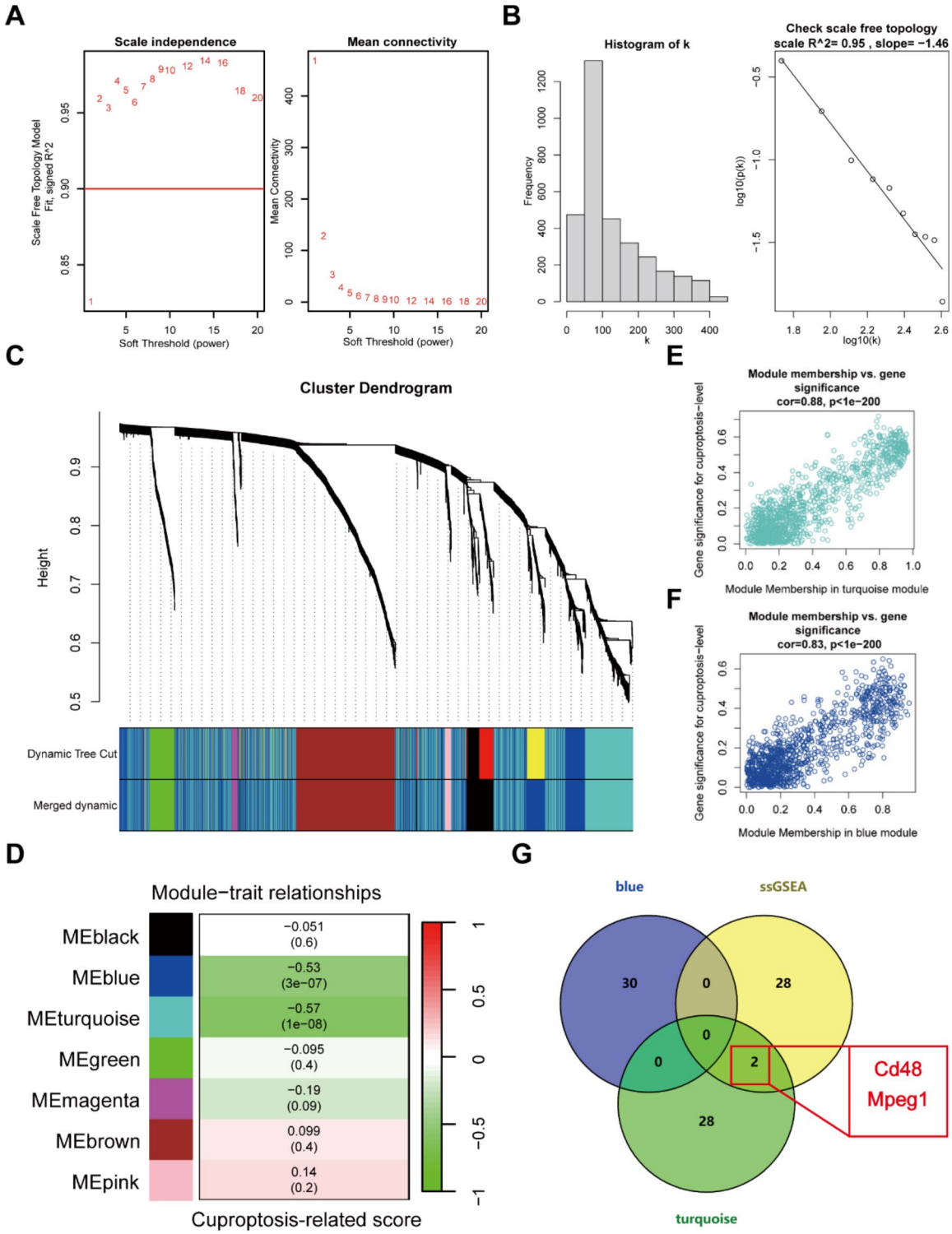

Fig. 4. Cuproptosis-related gene models of spinal cord injury. (**A**–**B**) The gene model was explored by co-expression analysis, and 2 was selected as the soft threshold. (**C**) Based on Spearman correlation coefficient, the heatmap of gene module-trait relationship was drawn to show the correlation. (**D**) Two gene models (MEturquoise, MEblue) were negatively associated with the cuproptosis-related score. Correlation results between module membership and gene significance for MEturquoise (**E**) and MEblue (**F**). (**G**) The results of cuproptosis-related DEGs and WGCNA were crossed to obtain two hub genes.

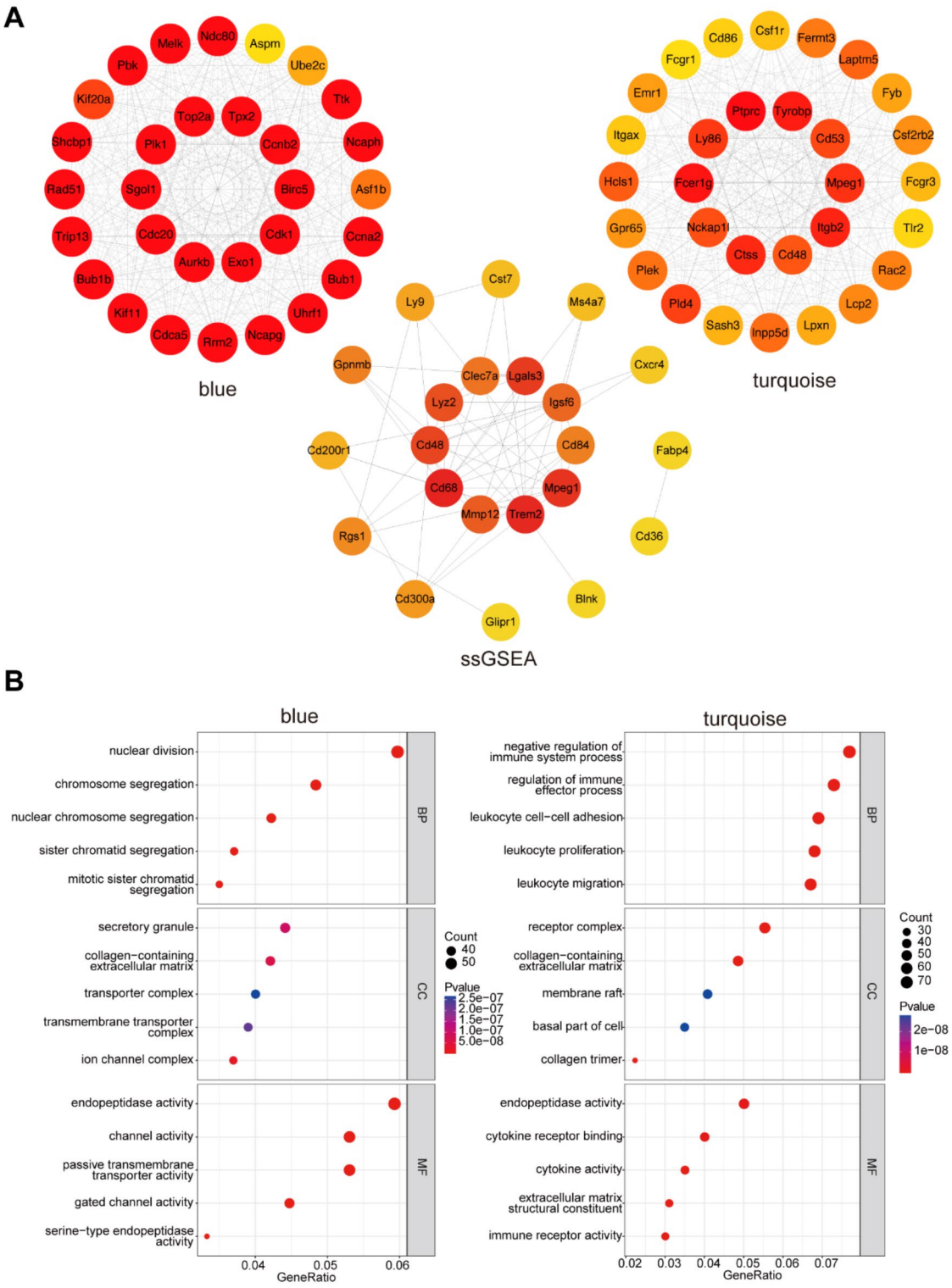

Fig. 5. Functional enrichment analysis of two gene model. (**A**) PPI network analysis results of top 30 cuproptosis-related DEGs, top 30 turquoise and blue module genes. (**B**) functional enrichment analysis was performed by combining all turquoise and blue module genes, respectively.

migration, etc. (Fig. 5B). This finding suggested that the turquoise module gene associated with cuproptosis might play a critical role in the immune regulation process of SCI.

Relationship between immune infiltration and cuproptosis in spinal cord injury

We commenced by employing seven algorithms to analyze the immune infiltration landscape associated with cuproptosis (Fig. S4). Figure 6A demonstrated that the NK cells, Centriole cells, and Plasma cells were enriched in high cuproptosis-related score group. Conversely, B cells, T cells, macrophages, and others were enriched in low cuproptosis-related score group (Fig. 6B).

Subsequently, building upon the results from the seven immune infiltration landscapes, we performed immune cell correlation analysis separately for *Cd48* and *Mpeg1* (Fig. 7A). A particularly noteworthy finding was that M2 macrophages displayed a positive correlation with both hub genes, whereas they exhibited a negative correlation with neutrophil infiltration. Then, single-gene GSEA found that *Cd48* and *Mpeg1* were involved in very similar pathways in SCI: both contain IL – 17 signaling pathway, Lysosome, Phagosome, etc. (Fig. 7B). This finding prompted us to investigate the correlation between the expression levels of these two hub genes and their association with cuproptosis-related genes. The results showed a very high positive correlation between *Cd48* and *Mpeg1* ($R = 0.92$). Conversely, most other cuproptosis-related genes exhibited a negative correlation with these two hub genes (Fig. 7C). This suggests that *Cd48* and *Mpeg1* may play a unique role in spinal cord injury and their expression levels may be regulated by different mechanisms than other cuproptosis-related genes. Further research is needed to elucidate this mechanism and determine the potential therapeutic significance of these two hub genes in spinal cord injury.

Single-cell analysis and in vitro study

In this study, we conducted a comprehensive analysis of a single-cell dataset obtained from SCI using the Seurat package. The UMAP algorithm was employed to transform the high-dimensional data into a two-dimensional plot, allowing us to visualize and identify distinct cell populations. A total of 12 clusters were identified, including neurons, astrocytes, microglia, endothelial cells, and others (Fig. 8A). We focused on the expression of *Cd48*

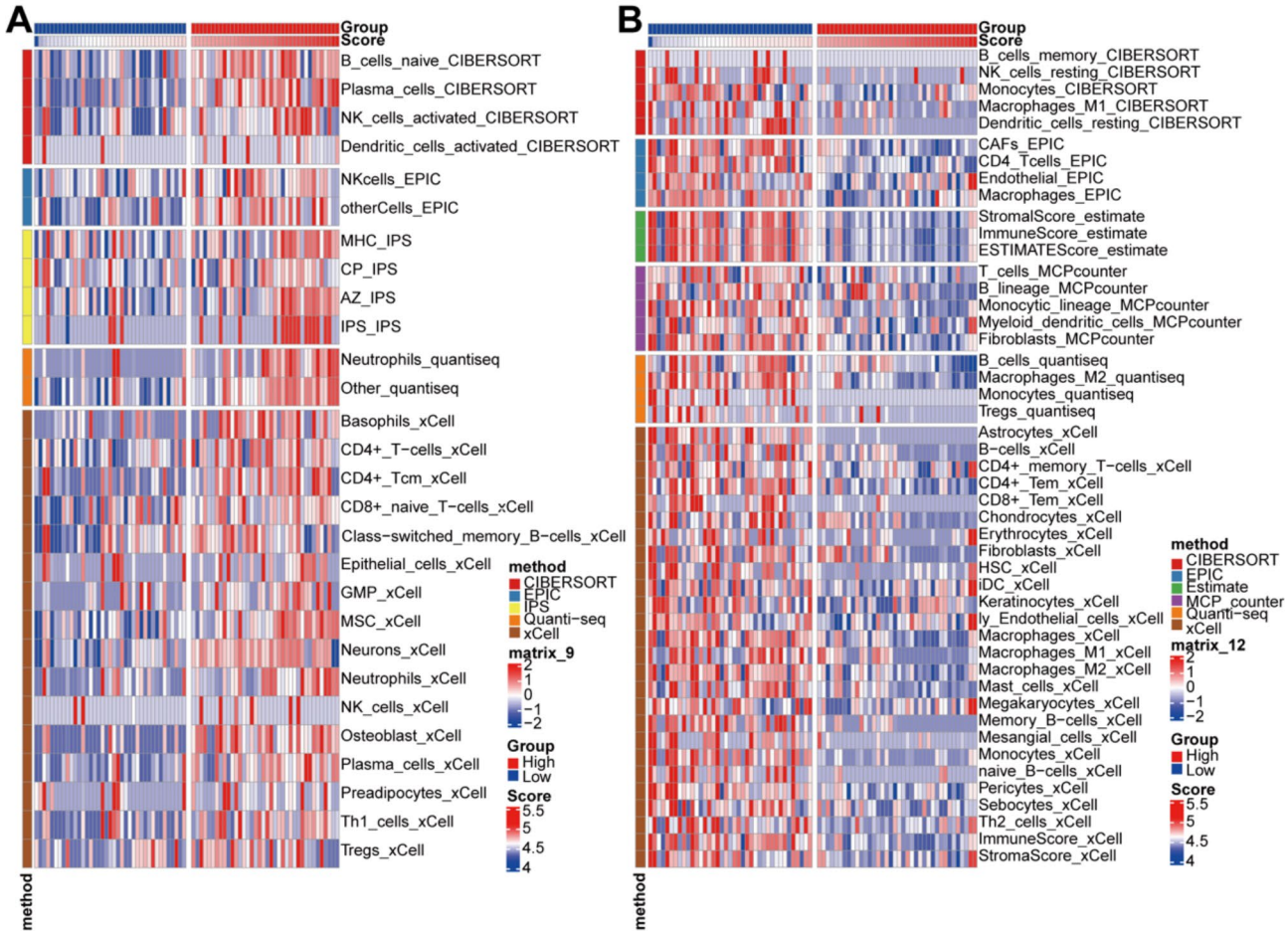

Fig. 6. Association between cuproptosis-related score and immune infiltration. The analysis of immune cell infiltration of up-regulated (**A**) and down-regulated (**B**) in the high-score group. Different colors on the left side of the heat map represent different immune infiltration algorithms, including CIBERSORT, ESTIMATE, IPS, MCPCOUNTER, XCELL, QUANTISEQ, MCP and EPIC.

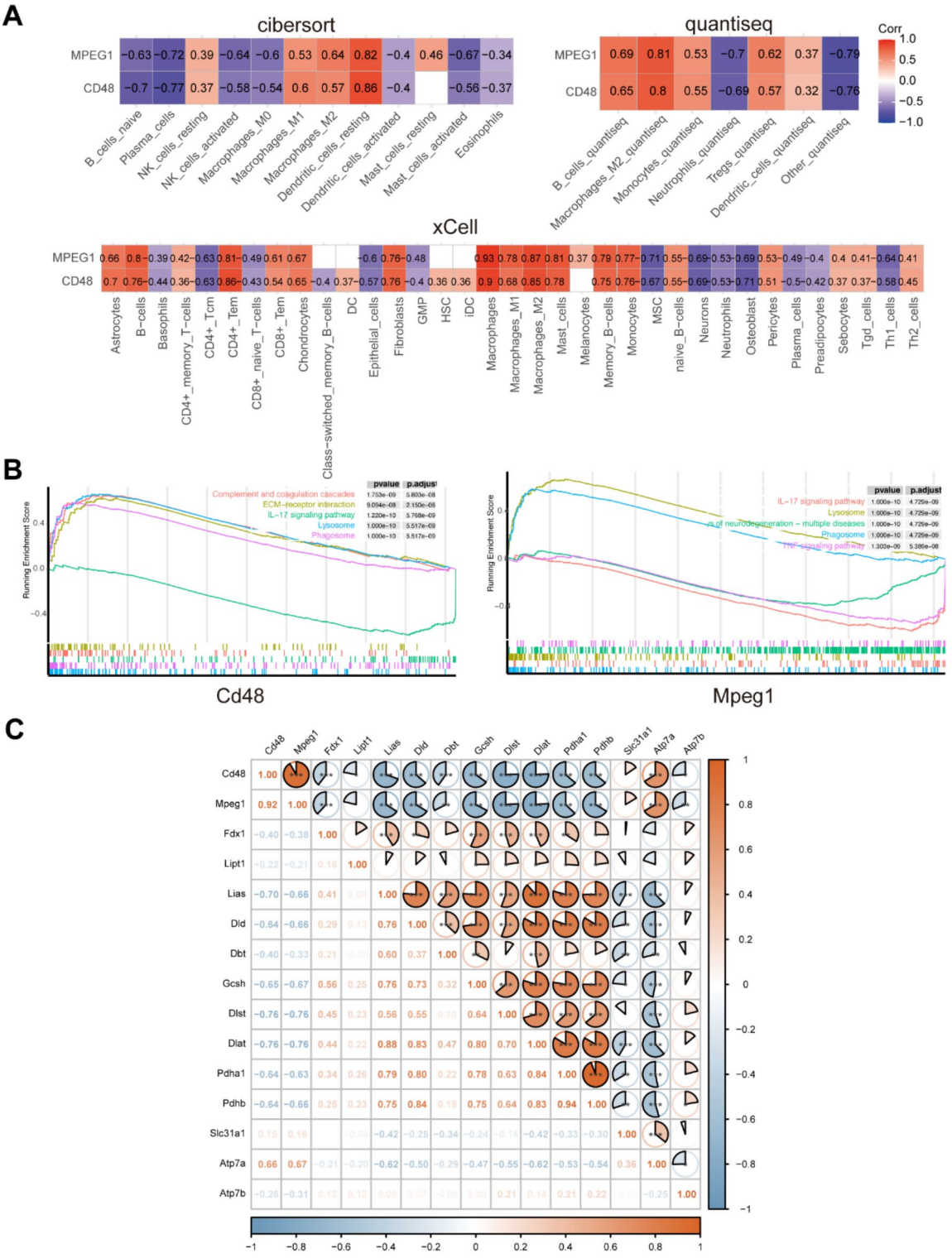

Fig. 7. The function of CD48 and MPEG1. (**A**) The correlation analysis of immune cell infiltration revealed that CD48 and MPEG1 could be co-expressed in specific macrophages and neutrophils. (**B**) GSEA of CD48 and MPEG1 showed significant enrichment of inflammatory pathways such as IL-17 signaling, as well as phagosomes and lysosomes. (**C**) Correlation analysis between CD48 and MPEG1 and cuproptosis marker genes. (*P<0.05, **P<0.01, and ***P<0.001).

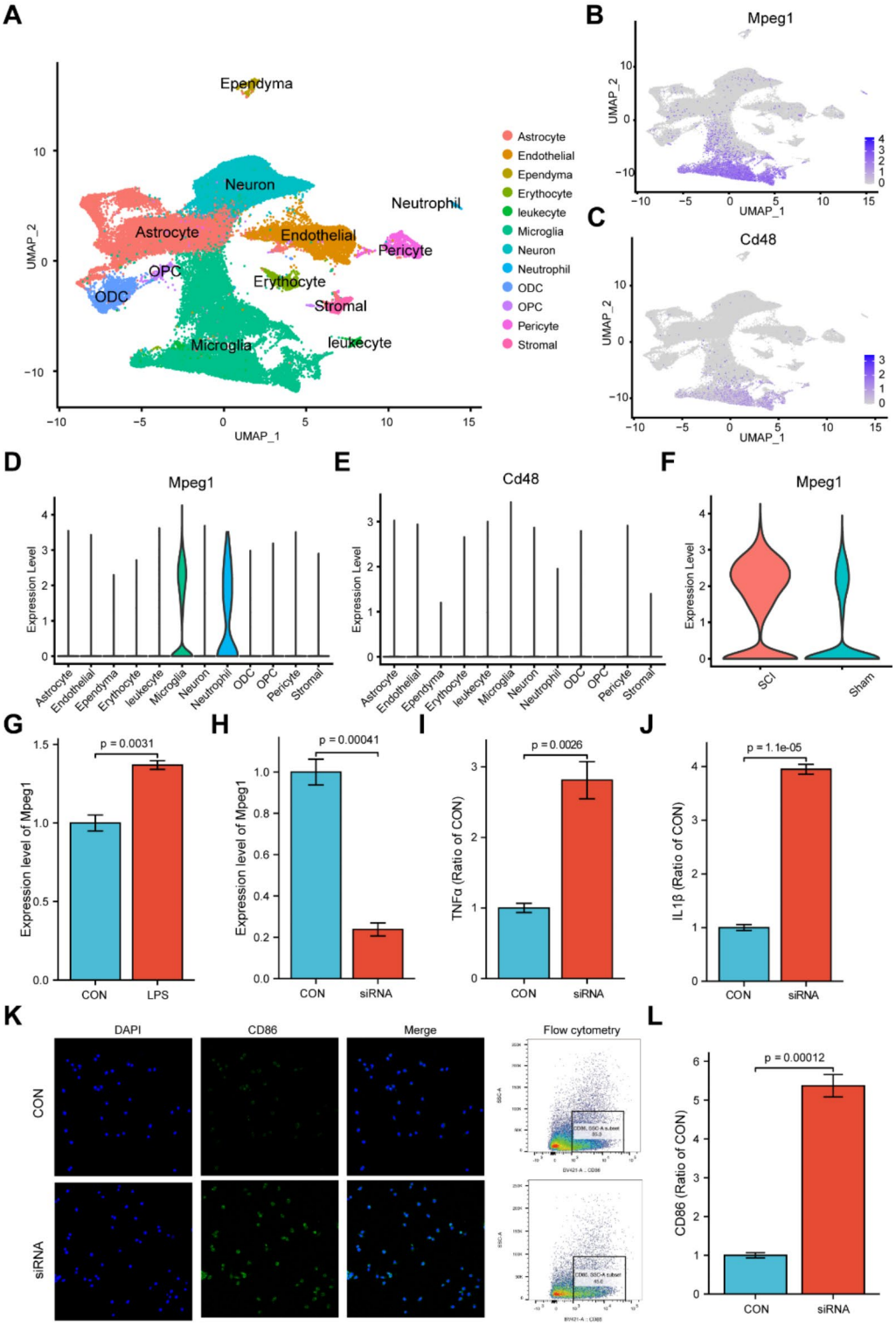

Fig. 8. Single-cell RNA sequencing analysis and validation of Mpeg1. (**A**) The UMAP plot depicts the major cell types identified through single-cell sequencing. (**B**) The UMAP plot displays the expression distribution of Mpeg1 in the major cell types. (**C**) The UMAP plot shows the expression distribution of Cd48 in the major cell types. (**D**) Violin plots of Mpeg1 protein expression in major cell types. (**E**) Violin plots of Cd48 protein expression in major cell types. (**F**) Violin plots of Mpeg1 expression in the spinal cord injury group compared to the sham surgery group. (**G**) Expression of Mpeg1 at the mRNA level in BV2 cell lines from the normal group and the LPS group. (**H**) siRNA successfully knockdown the level of Mpeg1. (**I**–**L**) Mpeg1 knockdown increased the TNFα, ILβ and CD86 level.

and *Mpeg1*. Interestingly, we found that microglia exhibited the highest expression levels of *Cd48* and *Mpeg1* compared to other cell types (Fig. 8B–E). This observation suggests that microglia may play a critical role in the context of spinal cord injury. Moreover, we observed that the expression levels of *Mpeg1* was elevated in the SCI group compared to the sham group (Fig. 8F). To further validate these findings, we performed qRT-PCR experiments in the BV2 cell line. Consistent with our bioinformatics analysis, the results demonstrated a significant increase in the mRNA levels of *Mpeg1* in the LPS group compared to the control group (Fig. 8G). To uncover the molecular functions of *Mpeg1*, siRNA was used to knockdown the *Mpeg1* (Fig. 8H). Then, the results showed that *Mpeg1* knockdown increased the inflammation level, characterized by the upregulation of inflammatory cytokines (TNFα, ILβ) and the level of M1 microglia marker (CD86). (Fig. 8I-L)

Discussion

Recent research had revealed that copper can directly bind to lipoylated components of the tricarboxylic acid (TCA) cycle and induce cell death, a process termed "cuproptosis"[12]. Cuproptosis is intricately associated with the onset, treatment, and prognosis of non-neoplastic conditions, such as Alzheimer's disease[26], inflammatory bowel disease (IBD)[27] and rheumatoid arthritis(RA)[28], as well as malignant diseases including bladder cancer[26], hepatocellular carcinoma[29] and lung adenocarcinoma[30]. Nevertheless, the role of cuproptosis, this emerging form of cell demise, has not yet been investigated in the context of SCI. Other forms of cell death akin to cuproptosis, such as ferroptosis[31,32] induced by extensive spinal cord hemorrhage, ROS activation, elevated glutamate excitotoxicity, and pyroptosis-regulated cell death mediated by NLRP3, have been demonstrated to play pivotal roles in SCI. Consequently, we embarked on an extensive exploration to address the following questions: Does cuproptosis indeed play a substantial role in SCI.

SCI severely impairs the transmission of nerve messages, resulting in profound consequences. Damage to the spinal cord at different levels can lead to sensory and motor dysfunction of varying degrees, and in severe cases, it may result in paralysis or even be life-threatening[33]. Following an SCI, there is often an imbalance in the microenvironment[33], which refers to the dysregulation of tissue, cellular, and molecular factors at different times and in different regions, further exacerbating the progression of SCI. Our research findings align with this perspective. We discovered a negative correlation between cuproptosis and immune cell infiltration. The enrichment analysis of the turquoise module obtained through WGCNA revealed that cuproptosis is involved in the negative regulation of the immune system and the chemotaxis of leukocytes. At the cellular level, the microenvironment imbalance involves the activation of astrocytes, differentiation of endogenous neural stem cells, oligodendrocyte progenitors, microglia, and infiltration of macrophages[33]. In addition, in the inflammatory cascade triggered by the interaction of immune cells, various immune cells such as monocytes, neutrophils, T lymphocytes, B lymphocytes, and macrophages invade the spinal cord tissue, congregating around the lesion core and releasing numerous inflammatory cytokines. While this response serves to limit the further expansion of the injury, it also prompts a robust immune reaction that exacerbates spinal cord tissue damage[34]. Our investigation further revealed a close relationship between hub genes *Cd48* and *Mpeg1* and a variety of immune cell infiltration as well as IL-17 cytokines. These findings highlight the intricate interplay between cuproptosis, immune cell responses, and inflammatory processes in the context of SCI. Further understanding of these mechanisms holds promise for the development of targeted therapeutic strategies aimed at mitigating the detrimental effects of SCI.

Cd48 and *Mpeg1* predominantly express on the surface of immune cells, playing essential roles in immune regulation and cell-cell interactions[21,35]. The activation of various immune cells and the ensuing inflammatory responses following SCI can lead to secondary injuries, exacerbating nerve tissue damage. Our investigation unveiled a strong positive correlation between both *Cd48* and *Mpeg1* with M2 macrophage infiltration, while displaying an inverse association with neutrophil infiltration. Furthermore, the analysis of single-cell RNA sequencing data and the validation through in vitro experiments substantiated the potential roles of *Mpeg1* in spinal cord injury. This may be related to the mouse samples we obtained from GEO, most of which belonged to early stage after SCI. During the early post-SCI period, infiltrated macrophages play a beneficial role in recognizing, phagocytosis and degradation of pathogens, apoptotic cells and tissue debris, and removal of inhibitory myelin components and cell debris, this promotes myelin regeneration and axon regrowth[36,37]. In addition, neutrophils are the first immune cells to arrive at the site of injury[38], and their infiltration within 3 h after SCI can have detrimental effects through the secretion of injury factors[39]. Studies in mice have shown that inhibiting neutrophil accumulation after SCI can enhance white matter retention and facilitate rapid nervous system recovery[40]. Consequently, *Mpeg1* appeared to have a favorable impact on SCI recovery.

Our research findings indicate that *Mpeg1* participated in several pathways in SCI and exhibit a strong negative correlation with cuproptosis-related genes. This implies that *Mpeg1* might be modulated to mitigate inflammation, decrease cell apoptosis, and reduce cytokine release in the early stages of SCI, thereby safeguarding spinal cord tissue from further harm. Nevertheless, the precise mechanisms underlying the involvement of *Mpeg1* in SCI's immune regulation necessitate extensive experimental validation. A prior study has indicated a decrease in *Mpeg1* expression during the acute phase of SCI[41], suggesting that *Mpeg1* may possess a potential regulatory role and serve as a beneficial receptor in SCI. The involvement of *Mpeg1* as immune regulatory molecules may provide a potential target for treating SCI, and further research can help uncover their precise roles and potential treatment strategies in spinal cord injury. Furthermore, through in-depth exploration of the interaction mechanisms between copper ions and immune cells, such as macrophages, neutrophils, and B cells, a more comprehensive understanding of the role of copper ions in cytotoxicity can be achieved.

Data availability

All databases used in this study were obtained from publicly available sources. Transcriptome data was obtained from four Gene Expression Omnibus (GEO) datasets: GSE42828, GSE47681, GSE27359, and GSE5296. Sin-

gle-cell sequencing data was retrieved from the following source: https://doi.org/10.6084/m9.figshare.17702045.v2.

Received: 4 September 2024; Accepted: 8 January 2025
Published online: 15 January 2025

References

1. Clifford, T., Finkel, Z., Rodriguez, B., Joseph, A. & Cai, L. Current advancements in spinal cord injury research-glial scar formation and neural regeneration. *Cells* **12**(6), 853. https://doi.org/10.3390/cells12060853 (2023).
2. McRae, J., Morgan, S., Wallace, E. & Miles, A. Oropharyngeal dysphagia in acute cervical spinal cord Injury: A literature review. *Dysphagia* **38**(4), 1025–1038. https://doi.org/10.1007/s00455-022-10535-0 (2023).
3. Ding, W. et al. Spinal cord Injury: The Global incidence, prevalence, and disability from the global burden of disease study 2019. *Spine (Phila Pa. 1976)* **47**(21), 1532–1540. https://doi.org/10.1097/BRS.0000000000004417 (2022).
4. Zhang, P., Liu, H., Sun, Z., Wang, J. & Wang, G. The application of O-arm and navigation system in precise localization of spinal cord lesions: A case series study. *Clin. Neurol. Neurosurg.* **196**, 105922. https://doi.org/10.1016/j.clineuro.2020.105922 (2020).
5. Wilson, J. R., Forgione, N. & Fehlings, M. G. Emerging therapies for acute traumatic spinal cord injury. *CMAJ* **185**(6), 485–492. https://doi.org/10.1503/cmaj.121206 (2013).
6. Anwar, M. A., Al Shehabi, T. S. & Eid, A. H. Inflammogenesis of secondary spinal cord Injury. *Front. Cell. Neurosci.* **10**, 98. https://doi.org/10.3389/fncel.2016.00098 (2016).
7. Schwab, M. E. & Strittmatter, S. M. Nogo limits neural plasticity and recovery from injury. *Curr. Opin. Neurobiol.* **27**, 53–60. https://doi.org/10.1016/j.conb.2014.02.011 (2014).
8. Tran, A. P., Warren, P. M. & Silver, J. New insights into glial scar formation after spinal cord injury. *Cell. Tissue Res.* **387**(3), 319–336. https://doi.org/10.1007/s00441-021-03477-w (2022).
9. Bradbury, E. J. & Burnside, E. R. Moving beyond the glial scar for spinal cord repair. *Nat. Commun.* **10**(1), 3879. https://doi.org/10.1038/s41467-019-11707-7 (2019).
10. Anjum, A. et al. Spinal cord injury: Pathophysiology, multimolecular interactions, and underlying recovery mechanisms. *Int. J. Mol. Sci.* **21**(20), 7533. https://doi.org/10.3390/ijms21207533 (2020).
11. Shi, Z. et al. Programmed cell death in spinal cord injury pathogenesis and therapy. *Cell. Prolif.* **54**(3), e12992. https://doi.org/10.1111/cpr.12992 (2021).
12. Tsvetkov, P. et al. Copper induces cell death by targeting lipoylated TCA cycle proteins. *Science* **375**(6586), 1254–1261. https://doi.org/10.1126/science.abf0529 (2022).
13. Wu, M. et al. Comprehensive analysis of the cuproptosis-related model to predict prognosis and indicate tumor immune infiltration in lung adenocarcinoma. *Front. Oncol.* **12**, 935672. https://doi.org/10.3389/fonc.2022.935672 (2022).
14. Lee, J. Y. et al. New novel mutation of the ATP7B gene in a family with Wilson disease. *J. Neurol. Sci.* **313**(1–2), 129–131. https://doi.org/10.1016/j.jns.2011.09.007 (2012).
15. Guo, H. et al. Copper induces spleen damage through modulation of oxidative stress, apoptosis, DNA damage, and inflammation. *Biol. Trace Elem. Res.* **200**(2), 669–677. https://doi.org/10.1007/s12011-021-02672-8 (2022).
16. Ge, E. J. et al. Connecting copper and cancer: From transition metal signalling to metalloplasia. *Nat. Rev. Cancer* **22**(2), 102–113. https://doi.org/10.1038/s41568-021-00417-2 (2022).
17. Qi, X. et al. The potential value of cuprotosis (copper-induced cell death) in the therapy of clear cell renal cell carcinoma. *Am. J. Cancer Res.* **12**(8), 3947–3966. https://doi.org/10.62347/ETJH6697 (2022).
18. Seelig, J. et al. Selenium and copper status: Potential signposts for neurological remission after traumatic spinal cord injury. *J. Trace Elem. Med. Biol.* **57**, 126415. https://doi.org/10.1016/j.jtemb.2019.126415 (2020).
19. Garcia, E. et al. Zinc, selenium, and copper re-establishes T-cell function and improves motor recovery in a rat model of spinal cord Injury. *Cell. Transpl.* **31**, 9636897221109884. https://doi.org/10.1177/09636897221109884 (2022).
20. Ebrahimnezhaddarzi, S. et al. Mpeg1 is not essential for antibacterial or antiviral immunity, but is implicated in antigen presentation. *Immunol. Cell. Biol.* **100**(7), 529–546. https://doi.org/10.1111/imcb.12554 (2022).
21. McCormack, R. M. et al. Perforin-2 is essential for intracellular defense of parenchymal cells and phagocytes against pathogenic bacteria. *Elife* **4**, e06508. https://doi.org/10.7554/eLife.06508 (2015).
22. Bayly-Jones, C., Pang, S. S., Spicer, B. A., Whisstock, J. C. & Dunstone, M. A. Ancient but not forgotten: New insights into MPEG1, a Macrophage perforin-like immune effector. *Front. Immunol.* **11**, 581906. https://doi.org/10.3389/fimmu.2020.581906 (2020).
23. Ferrero, G. et al. The macrophage-expressed gene (mpeg) 1 identifies a subpopulation of B cells in the adult zebrafish. *J. Leukoc. Biol.* **107**(3), 431–443. https://doi.org/10.1002/JLB.1A1119-223R (2020).
24. Zhang, C. et al. Identification of significant modules and hub genes involved in hepatic encephalopathy using WGCNA. *Eur. J. Med. Res.* **27**(1), 264. https://doi.org/10.1186/s40001-022-00898-3 (2022).
25. Zeng, F., Shi, M., Xiao, H. & Chi, X. WGCNA-based identification of hub genes and key pathways involved in nonalcoholic fatty liver disease. *Biomed. Res. Int.* **2021** 5633211. https://doi.org/10.1155/2021/5633211 (2021).
26. Lai, Y. et al. Identification and immunological characterization of cuproptosis-related molecular clusters in Alzheimer's disease. *Front. Aging Neurosci.* **14**, 932676. https://doi.org/10.3389/fnagi.2022.932676 (2022).
27. Chen, Y. et al. A broad cuproptosis landscape in inflammatory bowel disease. *Front. Immunol.* **13**, 1031539. https://doi.org/10.3389/fimmu.2022.1031539 (2022).
28. Zhao, J., Guo, S., Schrodi, S. J. & He, D. Cuproptosis and cuproptosis-related genes in rheumatoid arthritis: Implication, prospects, and perspectives. *Front. Immunol.* **13**, 930278. https://doi.org/10.3389/fimmu.2022.930278 (2022).
29. Zhang, G., Sun, J. & Zhang, X. A novel cuproptosis-related LncRNA signature to predict prognosis in hepatocellular carcinoma. *Sci. Rep.* **12**(1), 11325. https://doi.org/10.1038/s41598-022-15251-1 (2022).
30. Wang, F., Lin, H., Su, Q. & Li, C. Cuproptosis-related lncRNA predict prognosis and immune response of lung adenocarcinoma. *World J. Surg. Oncol.* **20**(1), 275. https://doi.org/10.1186/s12957-022-02727-7 (2022).
31. Chen, Y. et al. The latest view on the mechanism of ferroptosis and its research progress in spinal cord injury. *Oxid. Med. Cell Longev* **2020**, 6375938. https://doi.org/10.1155/2020/6375938 (2020).
32. Yao, X. et al. Deferoxamine promotes recovery of traumatic spinal cord injury by inhibiting ferroptosis. *Neural Regen Res.* **14**(3), 532–541. https://doi.org/10.4103/1673-5374.245480 (2019).
33. Fan, B. et al. Microenvironment Imbalance of spinal cord Injury. *Cell. Transpl.* **27**(6), 853–866. https://doi.org/10.1177/0963689718755778 (2018).
34. Deng, J. et al. Emerging roles of Microglia depletion in the treatment of spinal cord Injury. *Cells* **11**(12), 1871. https://doi.org/10.3390/cells11121871 (2022).
35. Pahima, H., Puzzovio, P. G. & Levi-Schaffer, F. 2B4 and CD48: A powerful couple of the immune system. *Clin. Immunol.* **204**, 64–68. https://doi.org/10.1016/j.clim.2018.10.014 (2019).
36. Van Broeckhoven, J., Sommer, D., Dooley, D., Hendrix, S. & Franssen, A. Macrophage phagocytosis after spinal cord injury: When friends become foes. *Brain* **144**(10), 2933–2945. https://doi.org/10.1093/brain/awab250 (2021).

37. Milich, L. M., Ryan, C. B. & Lee, J. K. The origin, fate, and contribution of macrophages to spinal cord injury pathology. *Acta Neuropathol.* **137**(5), 785–797. https://doi.org/10.1007/s00401-019-01992-3 (2019).
38. Tang, H. et al. The role of immune cells and associated immunological factors in the immune response to spinal cord injury. *Front. Immunol.* **13**, 1070540. https://doi.org/10.3389/fimmu.2022.1070540 (2022).
39. Zivkovic, S., Ayazi, M., Hammel, G. & Ren, Y. For Better or for worse: A look into neutrophils in traumatic spinal cord Injury. *Front. Cell. Neurosci.* **15**, 648076. https://doi.org/10.3389/fncel.2021.648076 (2021).
40. McCreedy, D. A. et al. Early Targeting of L-selectin on leukocytes promotes recovery after spinal cord injury, implicating novel mechanisms of pathogenesis. *eNeuro***5**(4), ENEURO.0101-18.2018. https://doi.org/10.1523/ENEURO.0101-18.2018 (2018).
41. Li, Q. et al. Identification of four genes and biological characteristics associated with acute spinal cord injury in rats integrated bioinformatics analysis. *Ann. Transl Med.* **9**(7), 570. https://doi.org/10.21037/atm-21-603 (2021).

Acknowledgements
We would like to express our heartfelt appreciation for the invaluable support and guidance provided by Chuan Chang and Yao Lv.

Author contributions
Conceptualization, C.C. and Y.L.; Data curation, D.M., Q.C.; Formal analysis, D.M., Q.C; Investigation, D.M., Q.C.; Methodology, D.M., Q.C.; Validation, D.M., Q.C., S.T., Z.X., and G.Y. Visualization, D.M., Q.C., S.T., Z.X., and G.Y.; Writing - original draft, D.M., Q.C., S.T., Z.X., and G.Y.; Writing - review & editing, C.C. and Y.L. All authors have read and agreed to the published version of the manuscript.

Funding
This research did not receive any specific grant from funding agencies in the public, commercial, or not-for-profit sectors.

Declarations

Competing interests
The authors declare no competing interests.

Additional information
Supplementary Information The online version contains supplementary material available at https://doi.org/10.1038/s41598-025-86170-0.

Correspondence and requests for materials should be addressed to C.C. or Y.L.

Reprints and permissions information is available at www.nature.com/reprints.

Publisher's note Springer Nature remains neutral with regard to jurisdictional claims in published maps and institutional affiliations.